Electrically Inhomogeneous Materials

Mat. Res. Soc. Symp. Proc. Vol. 699 © 2002 Materials Research Society R8.5

Electrical Characterization of Inhomogeneous and Heterogeneous Systems with Microstructural Periodicity

Joachim Maier
Max-Planck-Institut für Festkörperforschung, 70569 Stuttgart, Germany

ABSTRACT

This paper discusses how inhomogeneities and heterogeneities enter impedance and conductivity analyses in the case of microstructural periodicity. The specific considerations of various examples of ionically and ionically/electronically conducting materials systems (bicrystals, microcrystalline and nanocrystalline samples) show how a reliable and thorough characterization is possible.

INTRODUCTION

Realistic systems are at least partly inhomogeneous and heterogeneous corresponding to continuous or abrupt changes of the local electrical transport properties (e. g. at interfaces). This is particularly true for non-equilibrium systems exhibiting structural and/or compositional gradients. But also in equilibrium or partial equilibrium systems, heterogeneities (interfaces) and inhomogeneities (e. g. space charge zones) are ubiquitous. Since local changes in the transport parameters give rise to local and usually also to global electrical effects, local or global electrical measurements offer sensitive techniques for the determination of inhomogeneities or heterogeneities. The number of possibilities is inexhaustible, ranging from single crystals to percolative multiphase mixtures or artificially structured systems. Percolation and effective medium approaches, finite element and finite difference methods as well as resistor network techniques offer powerful description methods [1]. In this contribution we restrict ourselves to the treatment of systems which exhibit a certain microstructural periodicity such that the effects can be approximately described by a bricklayer approximation [2,3]. Even in cases in which the grain shape significantly deviates from a cubic shape and also in systems with a significant shape distribution, a bricklayer model may be valid to a remarkable degree. (The limits have been elaborated in Ref. [4].)

Even though special impedance techniques have been developed to obtain local resolution [5,6], we only consider the usual macroscopic impedance measurements in which serial impedances may show up according to the relaxation times as well as microimpedance techniques which allow for a certain space resolution.

INHOMOGENEITIES

Let us start with a single crystal subjected to a pseudo one-dimensional diffusion experiment resulting in a conductivity distribution along the x-axis, $\sigma(x, t)$. (Generally $\sigma(x, t)$ may be a complex function.) If the conductance (admittance) experiment is performed such that the measuring current flows perpendicular to the x-axis (in z-direction with electrode size $L_x \times L_y$ and electrode distance L_z), the differential conductance contributions $dx\sigma(x, t)L_y/L_z$ are connected in parallel and the conductance $R^{\|-1}$ is obtained by integration of the above

expression. Defining the effective conductivity $\sigma_m^{\parallel}(t)$ by $R^{\parallel -1} = \sigma_m(t)L_xL_y/L_z$ the result is

$$\sigma_m^{\parallel}(t) = \frac{1}{L_x}\int_0^{L_x}\sigma(x,t)dx. \quad (1)$$

If the experiment is performed along the x-axis we obtain, owing to the series-connection of the resistive elements $dx\sigma^{-1}(x,t)/L_yL_x$ and by defining an effective resistivity $\sigma_m^{\perp -1}$ by $L_x\sigma_m^{\perp -1}(t)/L_yL_z$,

$$\sigma_m^{\perp -1}(t) = \frac{1}{L_x}\int_0^{L_x}\sigma^{-1}(x,t)dx. \quad (2)$$

(Note that Eq. (2) is strictly valid only for a single carrier system or for carriers that are locally reversibly transformable [7].) The time dependence of the overall response can be used to determine the diffusion coefficient. Another possibility is to freeze-in a non-stationary profile (at $t = t_1$) and to resolve $\sigma(x,t_1)$ locally. Such a technique was used in Ref. [8] to detect the impurity diffusion coefficient of Cd^{2+} in AgCl. The principle of that method is that the impedance is not determined by the distance to the counter-electrode but by the diameter d of the tip of the working electrode. Owing to the current constriction only a limited small volume around the tip is probed and the conductivity of that volume detected:

$$R_{eff}(x) = \text{const}\frac{1}{\sigma(x,t)d} \quad (3)$$

(The value of const depends on the tip shape [9].)

In the above cases impedance measurements have been used to detect compositional effects. There are also situations in which inhomogeneities are *produced* by the impedance experiment [10]. This is the case when non-reversible electrodes are used, e. g. carbon or Pt in the case of mixed conducting Ag-electrolytes. While at high frequencies ions and electrons can move, at low frequencies the blocking nature of the electrode with respect to the ions becomes important. In the d. c. limit only electrons flow. The a. c. response is — to a first order approximation — characterized by a Warburg branch which corresponds to the $\sqrt{t}$ short-time behavior in the d. c. domain, followed by a semicircular part which corresponds to the long-time behavior in the d. c. domain. The maximum frequency is directly correlated with the chemical diffusion coefficient. Since usually such maximum frequencies are extremely small, the blocking technique is mostly performed as a d. c. experiment. An interesting variant is met if grain boundaries are selectively blocking. Then given a sufficient interfacial density, the relaxation time is significantly reduced [11]. Some examples to be addressed later refer to these issues.

At this point an apparent paradox shall be mentioned: If the mixed conductor is made purely ionically conductive by letting $\sigma_{eon} \longrightarrow 0$, an infinitely extended Warburg increase is predicted, while — if we had neglected σ_{eon} right from the beginning — a purely capacitive behavior (spike) would be expected. The solution of this dilemma lies in the ratio of electrical boundary capacitance [12] (which was neglected in the above consideration of the Warburg increase) and chemical capacitance which is decisive for the stoichiometry change. In Ref. [13] an equivalent circuit is given which allows a detailed understanding of the impedance in

electrically and/or chemically biased mixed conductive systems.

HETEROGENEITIES

Heterogeneities can be treated analogously by introducing steep $\sigma(x)$ profiles (in the limit: step functions). Usually such steps are met as a consequence of abrupt structural changes, e. g. at grain boundaries or at heterojunctions. There, not only the carrier concentrations but also the mobilities change; in addition, owing to the structural changes, charging effects occur which give rise to adjacent space charge regions. Hence heterogeneities usually imply local inhomogeneities. Before we tackle those systems explicitly, let us just recall that interfaces lying parallel to the measurement direction are electrically connected in parallel, whilst they are electrically connected in series if they have to be trespassed by the current. In this way, to be effective the first "type" of interfaces should be highly conductive whilst the second "type" requires an insulating nature. If we only have to consider parallel or serial switching, the effective values $\sigma_m^{\parallel}$ and $\sigma_m^{\perp -1}$ are given by (φ: volume fraction, β gives the portion of the grain boundary volume which is active in the direction indicated)

$$\begin{aligned} \sigma_m^{\parallel} &= \Sigma_\alpha \beta_\alpha^{\parallel} \varphi_\alpha \sigma_\alpha^{\parallel} \\ \sigma_m^{\perp -1} &= \Sigma_\alpha \beta_\alpha^{\perp} \varphi_\alpha \sigma_\alpha^{\perp -1}, \end{aligned} \tag{4}$$

respectively. As set out in Ref. [3], a general expression for the bricklayer model is given by (L denotes the boundary layer, ∞ denotes the bulk)

$$\hat{\sigma}_m = \left[\hat{\sigma}_\infty \hat{\sigma}_L^{\perp} + \beta_L^{\parallel} \varphi_L \hat{\sigma}_L^{\parallel} \hat{\sigma}_L^{\perp}\right] / \left[\hat{\sigma}_L^{\perp} + \beta_L^{\perp} \varphi_L \hat{\sigma}_\infty\right]. \tag{5}$$

Eq. (5) is an approximation the validity of which is inspected more closely in Ref. [14]. Here the complex quantity $\hat{\sigma}$ is used to allow for the description of the a. c. experiments, (see below). Eq. (5) which reduces to Eqs. (4) for $\sigma_{gb}^{\parallel} \to 0$ or $\sigma_{gb}^{\perp} \to \infty$, becomes important for high boundary fractions and particularly for systems in which the equation describes the superposition of three mechanisms: transport through the bulk ($\hat{\sigma}_\infty$), across the boundary ($\hat{\sigma}_{gb}^{\perp}$) and along the boundary ($\hat{\sigma}_{gb}^{\parallel}$).

For the purpose of illustration it is meaningful to assume distinctly different relaxation times ($\tau_L \ll \tau_\infty$) for boundary and bulk processes. The results [15] are

$$\hat{\sigma}_m = \hat{\sigma}_\infty + \frac{2}{3} \varphi_L \hat{\sigma}_L^{\parallel} \qquad \text{for } \omega \gg \tau_L^{-1} \tag{6a}$$

$$\hat{\sigma}_m^{-1} = \left(\sigma_\infty + \frac{2}{3} \varphi_L \sigma_L^{\parallel}\right)^{-1} + \frac{1}{3} \varphi_L \hat{\sigma}_L^{\perp -1} \qquad \text{for } \omega \ll \tau_\infty^{-1} \tag{6b}$$

As Eq. (5) these equations are also approximations with ranges of validity slightly different from Eq. (5) (see Ref. [14]). Eqs. (6) describe two semicircles in series belonging to the $\perp$-boundary and the parallel combination of bulk and $\parallel$-boundary (in the direction from low to high frequencies).

The situation becomes more complicated for selectively blocking grain boundaries [11] or very small grains [15–17]. Both contributions (resistive and highly conductive ones) can

occur in the same material. This can be possible if locally different interfaces are present, or since interfacial conductivities can be highly anisotropic. The anisotropy can have various reasons: the inhomogeneity of the space charge region, the different behavior of different carriers in the space charge regions as well as the sandwich character of the space charge zone core space charge zone composite.

SPACE CHARGE CONTAINING POLYCRYSTALS

In the following we consider the brick-layered polycrystal under (partial) equilibrium conditions. See Fig. 1. (If we "fill" the grain boundaries by dispersed second phase particles we have a reasonable picture of many composite systems of interest beyond the percolation limit.) The local mean contributions $\widehat{\sigma}_L^{\perp}$ and $\widehat{\sigma}_L^{\parallel}$ in Eq. (5) can be decomposed into

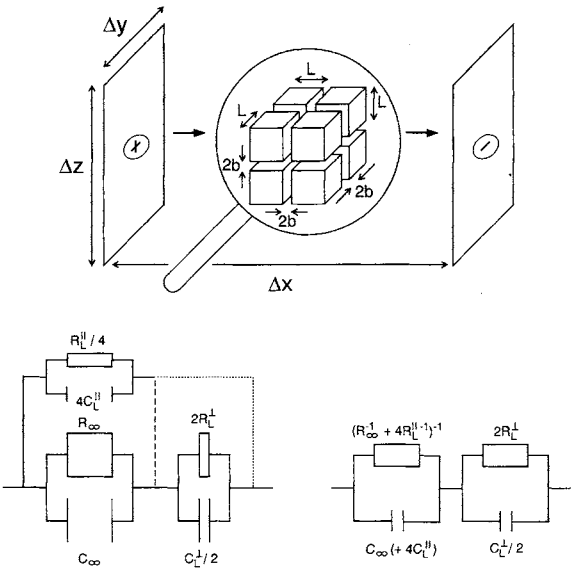

Figure 1: Schematic plot of a conductance experiment on a polycrystalline sample, where a greatly simplified grain topology is assumed (shown in magnification) and corresponding equivalent circuit according to Eqs. (6a, 6b) [3].

contributions stemming from the core (co) and from the space charge region (sc) (see Eq. (4)):

$$\begin{aligned} \widehat{\sigma}_{gb}^{\parallel} &= \varphi_{sc}\widehat{\sigma}_{sc}^{\parallel} + \varphi_{co}\widehat{\sigma}_{co}^{\parallel} \\ \widehat{\sigma}_{gb}^{\perp -1} &= \varphi_{sc}\widehat{\sigma}_{sc}^{\perp -1} + \varphi_{co}\widehat{\sigma}_{co}^{\perp -1}. \end{aligned} \tag{7}$$

The real parts of $\widehat{\sigma}_{sc}^{\parallel}$ and $\widehat{\sigma}_{sc}^{\perp}$ are obtained according to Eqs. (1, 2). The solution for various important cases is given in Table I. The capacitive elements of the $\perp$-components are substantial while the contributions of the $\parallel$-components are usually negligible.

The relations have to be modified in the sub-Debye regime when the space charges overlap [15,16]. Only in the limit of extremely small grains the space charge regions are

Table I: Possible space charge situations for acceptor doped (D′) metal rich oxides with oxygen vacancies and excess electrons as decisive carriers, and corresponding effective conductivity and resistivity expressions for electrons (n) and oxygen vacancies (V), respectively [18]. (c_{n0} and c_{v0} denote the respective boundary values (first layer adjacent to the core, and λ denotes the Debye length.)

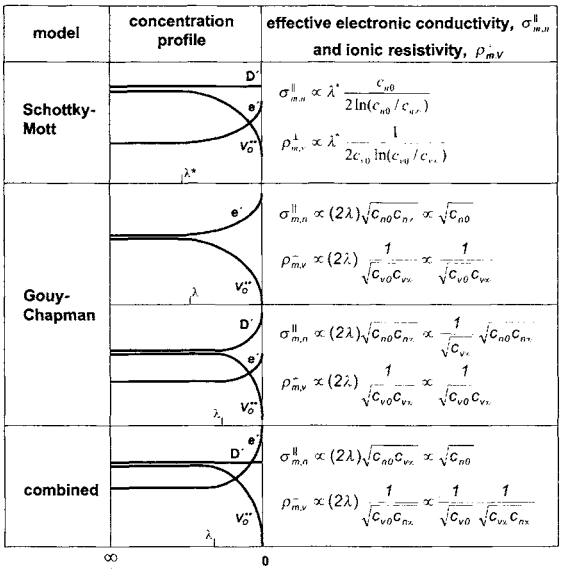

almost homogeneous with conductivities being characterized by a defect concentration c_0 throughout the sample.

Let us consider selected examples referring to AgCl, CaF_2, $SrTiO_3$ and CeO_2.

AgCl POLYCRYSTALS AND COMPOSITES

Figs. 2, 3 show the impedance response of a AgCl bicrystal and an AgCl polycrystal before and after annealing [3]. While the left semicircle refers to the Ag^+ bulk conductivity and the dielectric bulk constant, the right one yields the contact resistance which further investigations (capacitances) reveal to be a constriction resistance owing to bad contact. This right semicircle is significantly diminished by annealing. In the case of the polycrystal also two bulk semicircles are observed. However upon annealing, the right one decreases as in the bicrystal example, but the left one decreases. This is now clear evidence for the fact that two "types" of interfaces are to be distinguished: those forming the obstacles for Ag^+ bulk transport (serial boundaries) as well as those which short-circuit the bulk. Owing

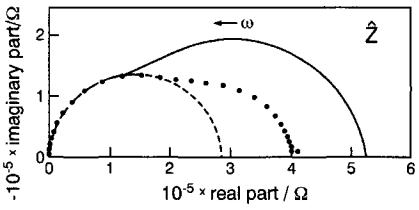

Figure 2: Impedance spectrum of an AgBr-crystal. The solid lines refer to the sample which has been heated to 96°C. After heating again to 190°C (1 h) and quenching to 96°C, the second semicircle diminishes (∗). After heating to 300°C (1 h) an cooling to 96°C, only the bulk semicircle remains (---), which is also obtained in a single-crystal experiment (half diameter) [19]. The cell constant in this experiment is 1.026 cm^{-1} [3].

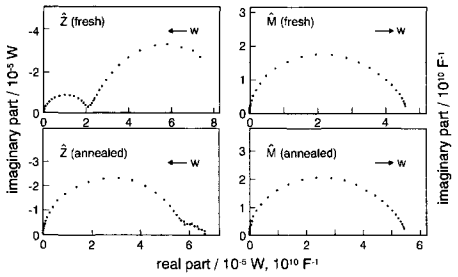

Figure 3: Plots of complex impedance and of complex inverse capacitance for a polycrystalline AgCl sample (25°C) before and after sintering (400°C) (cell constant: 0.076 cm^{-1}) [15,20].

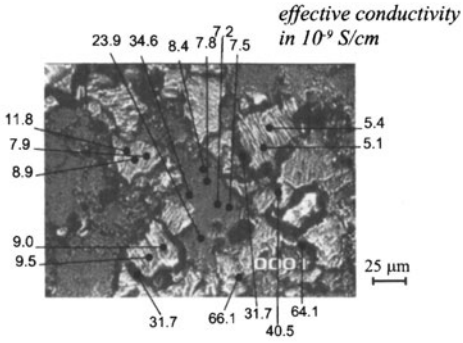

Figure 4: Microelectrode impedance spectroscopy reveals the higher conductivity of the grain boundaries compared to the bulk [21].

to accumulation layers (increased vacancy concentration) these parallel boundaries bypass the bulk. The invariance of the high frequency capacitance is displayed by the plots of the dielectric modulus (inverse capacitances form the intersections with the real axis) (see Fig. 1).

The highly conductive nature of the grain boundaries in AgCl is confirmed by microelectrode measurements (see Fig. 4) [8,22].

A similar equivalent circuit and a similar impedance response is obtained for AgCl:Al_2O_3 composites in which the very fine Al_2O_3 particles "fill" the grain boundaries and lead to much enhanced space charge effects [15].

The enhanced space charge potential is due to the basic nature of the Al_2O_3 surfaces according to [15]

$$Al_2O_3] + Ag_{Ag} \rightleftharpoons Al_2O_3]\,Ag^{\cdot} + V'_{Ag}. \tag{8}$$

ACTIVATED CaF_2 POLYCRYSTALS AND FLUORITE SUPERLATTICES

Related effects are observed for the anion conducting fluoride conductor CaF_2. Unlike in the previous example SiO_2 is more favorable owing to its comparatively acidic behavior:

$$SiO_2] + F_F \rightleftharpoons SiO_2]\,F' + V_F^{\cdot}. \tag{9}$$

This adsorption effect can also be induced by modifying grain boundaries by the super Lewis acids BF_3 or SbF_5, according to the tendency to form [23]

$$SbF_5 + F_F \rightleftharpoons SbF_6^- + V_F^{\cdot}. \tag{10}$$

Strong accumulation of $V_F^{\cdot}$ also explains the high conductivity of nanocrystalline CaF_2 [24]. Annealing such nanocrystalline CaF_2 leads to a grain size increase. Hence the high frequency semicircle of the impedance spectra enlarges significantly. The simultaneous increase of the low frequency semicircle can be attributed to the opening of large pores during grain growth.

Extreme conductivity effects also occur in composites of two ionic conductors such as AgCl:AgI. There we face the possibility of redistributing ionic defects over two space charge regions [15].

A very elegant experiment refers to the preparation of ionic superlattices of $BaF_2/CaF_2/BaF_2$..., whose "superlattice" constants were varied from 1 nm to 1μm. The increase of the

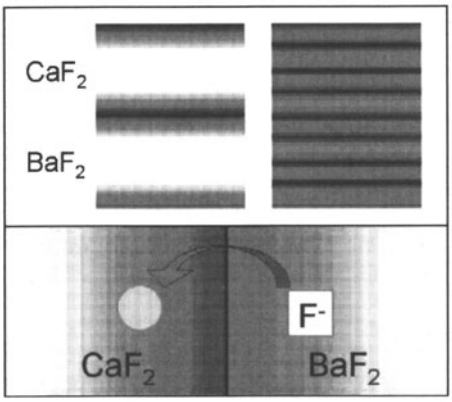

Figure 5: Ionic heterostructures composed of CaF_2 and BaF_2 leading to mesoscopic ion conduction.

conductivity with the number of heterojunctions, while the total volume of the two phases remains constant, is in quantitative agreement with a redistribution (see Fig. 5) according to [25]

$$F_F(BaF_2) + V_i(CaF_2) \rightleftharpoons F_i'(CaF_2) + V_F^{\cdot}(BaF_2). \tag{11}$$

The vacancies in BaF_2 seem to determine the conductivity of the packages at low T, while the interstitial defects in CaF_2 seem to take over at high T. The behavior at very small spacings indicate space charge overlap. All this refers to $\sigma_m^{\parallel}$; the measurement of $\sigma_m^{\perp}$ is under progress.

BICRYSTALLINE AND POLYCRYSTALLINE Fe-DOPED $SrTiO_3$

From electrical experiments on bicrystals we have detailed knowledge of depletion effects in Fe-doped $SrTiO_3$ [26–28] in relation to the type of the boundary. In a loose sense the segregation of positive charges increases with the structural difference of interfacial core and bulk and hence in the sequence

$$\Delta\phi(\Sigma 13) > \Delta\phi(\Sigma 5) > \Delta\phi(\Sigma 3). \tag{12}$$

The decreased hole concentration in the space charge zones gives rise to a clear grain boundary arc (with the expected bias dependence) in the bicrystal impedance ($\perp$ interface) (see Fig. 6). In polycrystals the overall grain boundary response as well as the response of the individual depletion layers have been measured by impedance and microimpedance (Fig. 7) techniques, respectively.

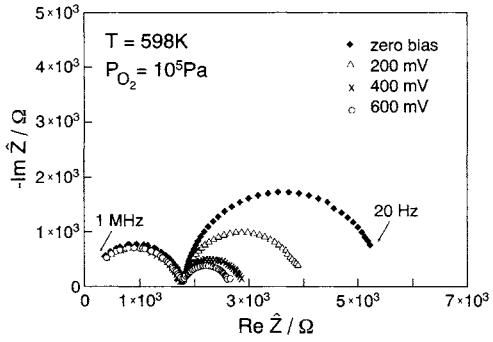

Figure 6: Impedance spectrum of a Fe-doped $SrTiO_3$ bicrystal [26].

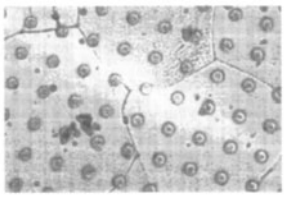

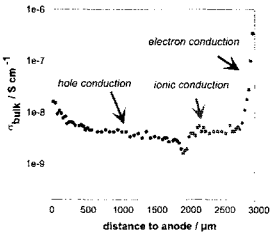

Figure 7: Cr/Au-microelectrodes with a diameter of 10μm evaporated on an iron-doped $SrTiO_3$ polycrystalline sample. The dark imprints of some electrodes are due to contacting with tungsten tips [29].